Tomi Mynttinen

A Switchable Double-line Phase Shifter and a Metamaterial Balun

Faculty of Electronics, Communications and Automation

Thesis submitted for examination for the degree of Master of Science in Technology.

Espoo 17.5.2010

Thesis supervisor:

Prof. Sergei Tretyakov

Thesis instructor:

Ph.D. Mikhail Lapine

Aalto University
School of Science
and Technology

Author: Tomi Mynttinen

Title: A Switchable Double-line Phase Shifter and a Metamaterial Balun

Date: 17.5.2010 Language: English Number of pages:7+48

Faculty of Electronics, Communications and Automation

Department of Radio Science and Technology

Professorship: Radio engineering Code: S-26

Supervisor: Prof. Sergei Tretyakov

Instructor: Ph.D. Mikhail Lapine

The goal of this work is to study the possibilities to create a wideband tunable phase shifter by using a new method with two loaded transmission lines to create the phase difference. Also a balun operating with the same principle is presented.

Both devices were designed using APLAC circuit simulator and the phase shifter was also realised into three samples. Both devices were designed to operate at UMTS frequency band, i.e. 1.92–2.17 GHz and the tunability range of the phase shifter was aimed to be at the range of $80°$–$100°$. Electronically controlled switched were used to tune the circuit.

The measurement results of the phase shifter show that with a few manufacturing iterations with homogeneous components it is possible to achieve precise phase shifts of, for instance, $80°$, $90°$ and $100°$. However, it seems that the switches used to manufacture the prototypes were unpredictable and difficult to simulate with available data.

According to the simulation results of the balun, it appears that this balun type is very sensitive to the type of the load. With some load types the output phase of the balun resonates in large measure, while with other loads the output phase is very stable in wide frequency ranges. However, further study is required to decide whether this is a usable approach.

Keywords: Phase shifter, power divider, microwave, balun, backward-wave, loaded transmission line

AALTO-YLIOPISTO

DIPLOMITYÖN
TIIVISTELMÄ

Tekijä: Tomi Mynttinen

Työn nimi: Säädettävä kaksoislinjavaiheensiirrin ja metamateriaalibaluni

Päivämäärä: 17.5.2010 Kieli: Englanti Sivumäärä:7+48

Elektroniikan, tietoliikenteen ja automaation tiedekunta

Radiotieteen ja -tekniikan laitos

Professuuri: Radiotekniikka Koodi: S-26

Valvoja: Prof. Sergei Tretyakov

Ohjaaja: FT. Mikhail Lapine

Tämän työn tavoitteena on tutkia uudentyyppisen laajakaistaisen vaiheensiirtimen säädettävyyttä eri vaiheensiirroille. Lisäksi esitellään samaan tenkiikkaan perustuva baluni.

Molemmat laitteet suunniteltiin ja simuloitiin käyttäen APLAC-piirisimulointiohjelmaa. Vaiheensiirtimestä valmistettiin lisäksi kolme prototyyppiä mittauksia varten. Molemmat laitteet suunniteltiin toimimaan UMTS-kaistalla, 1.92–2.17 GHz, ja vaiheensiirtimen säätöväliksi valittiin $80°$–$100°$. Säätäminen tapahtuu kytkinten avulla.

Vaiheensiirtimen mittaustulokset osoittavat, että tämän työn vaiheensiirrin-prototyyppien valmistuksessa käytettyjen kytkinten simulointi osoittautui hankalaksi. Tasalaatuisia komponentteja käyttäen on kuitenkin mahdollista valmistaa saman vaihe-eron tuottavia näytteitä.

Balunin simulaatiotulokset näyttävät olevan herkkiä balunin kuorman tyypille. Joillakin kuormilla balunin ulostulon vaihe resonoi voimakkaasti, kun taas toisilla ulostulovaihe on hyvin stabliili laajalla kaistalla. Balunin todellisen käyttökelpoisuuden selvittämiseksi vaaditaan tätä työtä laajempaa tutkimusta.

Avainsanat: Vaiheensiirrin, tehonjakaja, mikroaalto, baluni, paluuaalto, kuormattu siirtojohto

Preface

I want to thank my supervisor Prof. Sergei Tretyakov, instructor Ph.D. Mikhail Lapine and all the staff of the Department of Radio Science and Engineering for their expertise and help with this work.

I would also like to thank my family and friends for the help and support during this time period.

Otaniemi, 17.5.2010

Tomi O. Mynttinen

Contents

Symbols and Abbreviations

Symbols

$\mathbf{B}$	magnetic flux density
β	propagation constant
β_{TL}	propagation constant in a transmission line
C	capacitance
$\mathbf{D}$	electric displacement vector
d	length of a transmission line
$\mathbf{E}$	electric field
$\mathbf{E_0}$	complex electric field amplitude for a plane wave
ϵ	electric permittivity
ϵ_r	relative permittivity of a substrate
$\mathbf{H}$	magnetic field strenght
$\mathbf{H_0}$	complex magnetic field amplitude for a plane wave
h	thickness of a substrate
I	electric current
$\mathbf{J}$	electric current density
j	imaginary unit
$\mathbf{k}$	wave vector
L	inductance
μ	magnetic permeability
$\mathbf{r}$	position vector
ω	angular frequency
ω_{m}	matching angular frequency
ω_{op}	optimal operation frequency
ϕ	phase shift
ρ	electric charge density
ρ_n	normalized resistivity
$\mathbf{S}$	Poynting vector
T	transmitted amplitude
t	time or microstrip thickness
$\tan\delta$	substrate loss tangent
V_{on}	switch on -voltage $= 3.0\text{V}$
V_{off}	switch off -voltage $= 0.0\text{V}$
v_{ph}	phase velocity
ξ	proportionality coefficient
Z	impedance
Z_{in}	input impedance

Operators

$\nabla \times \mathbf{A}$	curl of vector $\mathbf{A}$
$\dfrac{\mathrm{d}}{\mathrm{d}t}$	derivative with respect to t
$\dfrac{\partial}{\partial t}$	partial derivative with respect to t
$\mathbf{A} \times \mathbf{B}$	cross product of vectors $\mathbf{A}$ and $\mathbf{B}$
$\mathbf{A} \cdot \mathbf{B}$	scalar product of vectors $\mathbf{A}$ and $\mathbf{B}$
$\Im\{a\}$	imaginary part of complex number a
$\Re\{a\}$	real part of complex number a
$\mathbf{A}^*$	complex conjugate of $\mathbf{A}$
$\arg(z)$	argument of z

Abbreviations

APLAC	an object-oriented analog circuit simulator and design tool
BW	backward wave
CPW	coplanar wave guide
DC	direct current
DLPS	double-line phase shifter
FW	forward wave
FW-BW-TL	forward- backward-wave transmission line
MESFET	metal epitaxial semiconductor field effect transistor
NRI	negative refraction index
SRR	split-ring resonator
TL	transmission line
UMTS	universal mobile telecommunications system

1 Introduction

Recently, rapidly increasing requirements for data transmission have led to the need for more broadband radio frequency devices. The wider the bandwidth, the more information can be carried. Since inventing the telegraph, the bandwidths of data transmission systems have increased exponentially. The transmitted data has developed from simple Morse code signal traveling through a wire, via speech, music and moving pictures to wireless transmission of many Mbit/s of data in the 3rd generation cellular radio systems. Due to this trend the need for more broadband components for new applications is naturally also high.

One of these components is phase shifter. Phase shifter is a device, which changes the phase angle of a signal propagating through it. A good phase shifter should have low losses, high power handling capacity, good matching and stable phase shift in a wide frequency band. Usually, also phase tunability is required. Phase tuning can be either continuous (analog phase shifters) or discrete (digital phase shifters).

Metamaterials have become important area of research in electromagnetics starting from early 2000s. Metamaterials are artificial materials, which obtain their material properties both from their structure and from the materials they are composed of. With these composite materials it is possible to achieve very special effective material properties, which are not met in natural materials.

One example of a metamaterial is the so called *backward-wave material* (or BW-material) in which the electromagnetic wave has the phase velocity in the opposite direction than the group velocity. This phenomenon is achieved when both permittivity ϵ and permeability μ of the material are negative. The applications of this particular metamaterial include the perfect lens which is based on the negative refractive index of such material.

The goal of this thesis is to design and measure a switchable *double-line phase shifter*

(or DLPS) [1], which uses the abilities of BW-metamaterials. This DLPS should have input and output impedance of $50\ \Omega$ and three switchable discrete phase shift positions of $80°$, $90°$ and $100°$ at Universal Mobile Telecommunications System (UMTS) frequency band, 1.92–2.17 GHz.

Chapter 2 is a literature review to introduce the reader to the theory, on which this novel application is based on, and what problems more traditional phase shifters have. Chapter 3 concentrates on the development of the DLPS and Chapter 4 shows the results of the work.

2 Literature Review

2.1 Basic Electromagnetics

The Maxwell's equations can be written as [10, 11]:

$$\nabla \cdot \mathbf{D} = \rho, \tag{2.1}$$

$$\nabla \cdot \mathbf{B} = 0, \tag{2.2}$$

$$\nabla \times \mathbf{E} = -\frac{\partial \mathbf{B}}{\partial t} \tag{2.3}$$

and

$$\nabla \times \mathbf{H} = \mathbf{J} + \frac{\partial \mathbf{D}}{\partial t}. \tag{2.4}$$

In linear and isotropic media

$$\mathbf{D} = \epsilon \mathbf{E} \ , \tag{2.5}$$

$$\mathbf{B} = \mu \mathbf{H} \ . \tag{2.6}$$

If the fields are time-harmonic, that is, if they oscillate at a constant frequency, they can be expressed as follows:

$$\mathbf{E}(\mathbf{r}, t) = \Re\{\mathbf{E}(\mathbf{r}) e^{j\omega t}\}, \tag{2.7}$$

$$\mathbf{H}(\mathbf{r}, t) = \Re\{\mathbf{H}(\mathbf{r}) e^{j\omega t}\}. \tag{2.8}$$

Substituting (2.7) and (2.8) into Maxwell's equations (2.1)–(2.4) leads to time-harmonic Maxwell's equations:

$$\nabla \cdot \mathbf{D} = \rho, \tag{2.9}$$

$$\nabla \cdot \mathbf{B} = 0, \tag{2.10}$$

$$\nabla \times \mathbf{E} = -j\omega \mathbf{B} \tag{2.11}$$

and

$$\nabla \times \mathbf{H} = \mathbf{J} + j\omega \mathbf{D}. \tag{2.12}$$

For a time-harmonic plane wave, the electric and magnetic field vectors are of the form

$$\mathbf{E}(\mathbf{r}) = \mathbf{E}_o e^{-j\mathbf{k}\cdot\mathbf{r}} \,, \tag{2.13}$$

$$\mathbf{H}(\mathbf{r}) = \mathbf{H}_o e^{-j\mathbf{k}\cdot\mathbf{r}} \,. \tag{2.14}$$

Substituting these into the time-harmonic Maxwell's curl equations (2.11) and (2.12) gives

$$\mathbf{H}_o = \frac{\mathbf{k}}{\omega\mu} \times \mathbf{E}_o \,, \tag{2.15}$$

$$\mathbf{E}_o = -\frac{\mathbf{k}}{\omega\epsilon} \times \mathbf{H}_o \,, \tag{2.16}$$

which can be combined into

$$\mathbf{E}_o = -\frac{1}{\omega^2\mu\epsilon}\mathbf{k} \times (\mathbf{k} \times \mathbf{E}_o) = -\frac{1}{\omega^2\mu\epsilon}[\mathbf{k}(\mathbf{k}\cdot\mathbf{E}_o) - \mathbf{E}_o(\mathbf{k}\cdot\mathbf{k})] \,. \tag{2.17}$$

Since $\mathbf{k}\cdot\mathbf{E}_o = 0$, (2.17) gives

$$\mathbf{k}\cdot\mathbf{k} = \omega^2\mu\epsilon \,, \tag{2.18}$$

which is called *the dispersion equation*.

2.2 Metamaterials

Although in this work volumetric *metamaterials* are not directly involved, their basic theory is worth discussing, because we will use loaded transmission lines mimicing their properties.

Metamaterials are artificial periodic structures, constructed of small (compared to the wavelength) building blocks. The shape, size and structure of these small particles determine the effective properties of these materials. These building blocks can be of any nature as long as they are electrically small. They may be represented by metallic C-shaped *split ring resonators* (SRR), pieces of thin wires, conductive or dielectric spheres or transmission-line grids loaded with lumped components. Due to this wide variety of possible solutions, metamaterials are capable of having very special electromagnetic characteristics, which makes them very interesting in designing novel applications in the areas of electromagnetism, optics and radio technology.

In particular, with metamaterials one can realize a so called *backward-wave* (or BW) material (also known as *negative refraction index* (NRI) or *double negative* material) discussed by V. G. Veselago already in 1968 [2]. In a BW-material both ϵ and μ are negative, which causes the phase velocity of the wave point in the opposite direction than the group velocity. This can be checked with the Poynting vector:

$$\mathbf{S} = \frac{1}{2}\Re\{\mathbf{E} \times \mathbf{H}^*\} = \frac{1}{2}\Re\{\mathbf{E}_o e^{-j\mathbf{k}\cdot\mathbf{r}} \times \mathbf{H}_o^* e^{j\mathbf{k}\cdot\mathbf{r}}\} = \frac{1}{2}\Re\{\mathbf{E}_o \times \mathbf{H}_o^*\} \ . \tag{2.19}$$

If μ and ϵ are negative in (2.15) and (2.16), i.e. $\mu \rightarrow -\mu$ and $\epsilon \rightarrow -\epsilon$, these equations become

$$\mathbf{H}_o = -\frac{\mathbf{k}}{\omega\mu} \times \mathbf{E}_o \ , \tag{2.20}$$

$$\mathbf{E}_o = \frac{\mathbf{k}}{\omega\epsilon} \times \mathbf{H}_o \ . \tag{2.21}$$

The dispersion equation (2.18) remains the same as for positive μ and ϵ, but substituting (2.20) into (2.19) gives

$$\begin{aligned} \mathbf{S} &= \frac{1}{2}\mathbf{E}_o \times (-\frac{\mathbf{k} \times \mathbf{E}_o^*}{\omega\mu}) = -\frac{1}{2\omega\mu}[(\mathbf{E}_o \cdot \mathbf{E}_o^*)\mathbf{k} - (\mathbf{E}_o \cdot \mathbf{k})\mathbf{E}_o^*] \\ &= -\frac{1}{2\omega\mu}|\mathbf{E}_o|^2\mathbf{k} \ , \end{aligned} \tag{2.22}$$

which indicates that the energy of the wave indeed propagates in the opposite direction than its phase.

This phenomenon has given rise to many new applications, for instance J.B. Pendry's *perfect lens* [3], miniaturized resonators and antennas, absorbers, tunable devices, etc. In this thesis, we will use backward-wave lines in phase shifter design.

2.3 Phase Shifters

2.3.1 Traditional Phase Shifters

There are many different types of phase shifters, which can be divided in four distinct groups [4] by their operational principle. These groups are:

- Transmission phase shifters

- Reflection phase shifters
- Loaded-line phase shifters
- Amplifying phase shifters

Transmission phase shifters — also referred to as switched line phase shifters — consist of two phase delaying transmission lines, a reference arm and a delay arm, which have electrically different lengths l_1 and l_2. The phase difference between these lines is then $\Delta\Phi = \beta(l_1 - l_2)$, in which β is the propagation factor of the lines. Instead of transmission lines, also phase delaying circuits can be used to reach the needed phase difference.

In reflection phase shifters a coupler or circulator along with reflective load is used to create a phase difference between input and output ports. For instance, the current, fed to port 1 of an isolator is reflected of a diode connected in port 2 and then comes out with a certain phase difference from port 3.

Loaded-line phase shifters are based on phase perturbation caused by a shunt load in a transmission line. To minimize the amplitude perturbation, another load a quarter-wavelength apart from the other is needed.

In amplifying phase shifters the phase shift can be usually achieved by using MESFETs (Metal Epitaxial Semiconductor Field Effect Transistor) as voltage controlled amplifiers.

The standard delay-line phase shifter with its linear frequency-phase dependency is very narrowband. Attempts of making broadband phase shifters with traditional methods has proven to be rather difficult. Such devices often end up being quite large or complex in structure. For excample, although in [5] the charasterictics of the designed phase shifter are reasonably good, the size of the device makes it impractical even if it is not tunable (see Figure 2.1).

In [6], the components were realized in a strip-transmission-line configuration consisting of three layers of dielectric with conducting strips located at the interfaces and

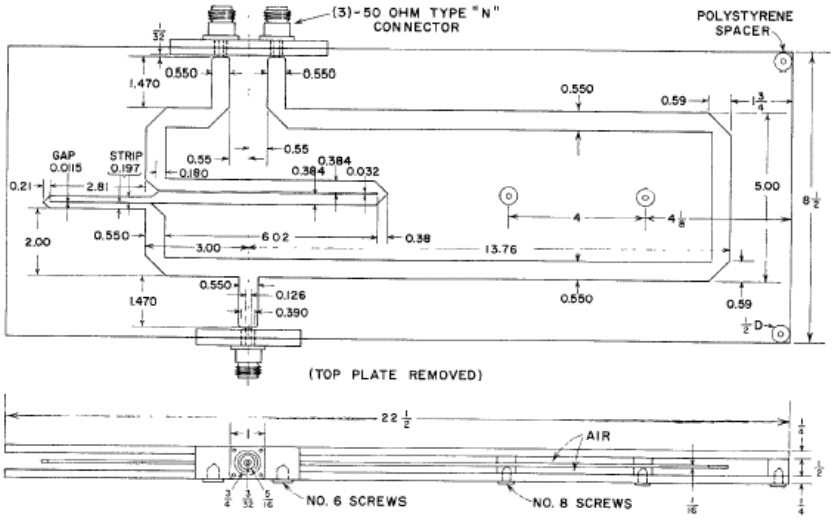

Figure 2.1: Experimental phase shifter by B. M. Schiffman for 300-1500 MHz frequency band. Dimensions in inches [5].

ground planes on the outer surfaces. Variation in coupling was achieved by displacing the strips along the interfaces.

The principal practical problem with these components was the reactive discontinuity at the junction between coupled sections of different coupling coefficients. It is the discontinuity which places a limit on the highfrequency operation of the components. In order to minimize these junction effects, one is forced to reduce the scale of the transmission-line cross section. The resulting smaller dimensions, however, result in increased attenuation and larger errors due to tolerances.

Report [7] presents the design and experimental results of a wide bandwith monolithic reflection-type phase shifter using a *coplanar waveguide* (CPW) Lange coupler, inductances and tunable capacitances fabricated on *barium strontium titanite* (BST). This design resulted in small size and good performance.

2.3.2 Novel Metamaterial Phase Shifters

In [8] a new type of phase shifter was introduced. It proposed the use of cascaded sections of negative refraction index transmission lines and positive refraction index transmission

lines, which offers some advantages over conventional delay lines and uniform backward-wave L-C lines. This kind of phase shifter is compact in size, esaily fabricated and exhibits a linear phase response around the operating frequency. According to the developers, it can produce either negative or positive phase shift values. However, in [9] it was proven that any combination of a forward- and backward-wave sections that produce positive phase shift is less broadband than a conventional transmission-line section with the same phase shift. Also, this solution is restricted to phase shifts around 180° and thus they cannot be used for arbitrary phase shifts.

The combined *forward- backward-wave transmission line* (FW-BW-TL) can be realized by combining normal transmission lines with series capacitors and shunt inductors. One unit cell of such one-dimensional "material" is shown in Fig. 2.2. Transmission

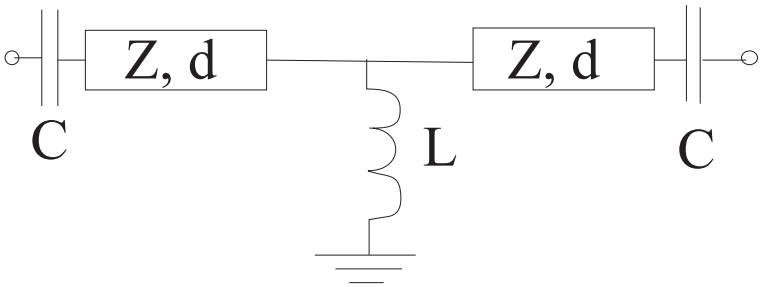

Figure 2.2: Unit cell of FW-BW-TL

matrix for such unit cell can be derived in the following way.

The transmission matrix of a normal transmission-line section is

$$A_{\mathrm{TL}} = \begin{pmatrix} \cos\beta_{\mathrm{TL}}d & jZ\sin\beta_{\mathrm{TL}}d \\ \frac{j\sin\beta_{\mathrm{TL}}d}{Z} & \cos\beta_{\mathrm{TL}}d \end{pmatrix} , \tag{2.23}$$

in which Z is the charasteristic impedance of the transmission line and β_{TL} is the propagation constant of the transmission line.

For a series capacitor and a shunt inductor the corresponding matrices are

$$A_{\mathrm{C}} = \begin{pmatrix} 1 & \frac{1}{j\omega C} \\ 0 & 1 \end{pmatrix} \tag{2.24}$$

and

$$A_{\mathrm{L}} = \begin{pmatrix} 1 & 0 \\ \frac{1}{j\omega L} & 1 \end{pmatrix} . \tag{2.25}$$

The transmission matrix for the whole unit cell is

$$A = A_{\mathrm{C}} \cdot (A_{\mathrm{TL}} \cdot (A_{\mathrm{L}} \cdot (A_{\mathrm{TL}} \cdot A_{\mathrm{C}}))) \ . \tag{2.26}$$

Let us then write the resulting matrix as

$$A = \begin{pmatrix} a_{11} & a_{12} \\ a_{21} & a_{22} \end{pmatrix} \ . \tag{2.27}$$

The input impedance for a perfectly matched FW-BW-TL can then be expressed as

$$Z_{\mathrm{in}} = \frac{(a_{11} - a_{22}) \pm \sqrt{(a_{11} - a_{22})^2 + 4a_{12}a_{21}}}{2a_{21}} \ . \tag{2.28}$$

In (2.28) the sign of the square root must be chosen so, that Re $Z_{\mathrm{in}} \geq 0$. Now, the phase shift along the BW-FW-TL can be written as

$$\phi = \arg\left(\frac{1}{a_{11} + \frac{a_{21}}{Z_{\mathrm{in}}}}\right) \tag{2.29}$$

and the transmission coefficient as

$$T = \left|\frac{1}{a_{11} + \frac{a_{21}}{Z_{\mathrm{in}}}}\right| \ . \tag{2.30}$$

The charasteristic impedance of the forward wave transmission line sections must be matched to the backward wave L-C arrangement. Thus

$$Z = \sqrt{\frac{L}{C}} \ . \tag{2.31}$$

This condition ensures, that there will be no additional band gap in the combined line. Forward and backward bands merge at the matching frequency

$$\omega_m^2 = \frac{1}{2}\frac{1}{\sqrt{LC}}\frac{v_{\mathrm{ph}}}{d} \ , \tag{2.32}$$

in which v_{ph} is the phase velocity in the transmission line segments and d is the length of one segment. Above this frequency the combined line operates as a forward-wave transmission line, while below this frequency it operates as a backward-wave transmission line.

To calculate the optimal values for a double-line phase shifter (DLPS) forward- backward-wave transmission line (FW-BW-TL) pairs, Ph.D. Mikhail Lapine has written a matlab code, which is shown in Appendix A.

The *double-line phase shifter* (DLPS) can be thought to be a transmission phase shifter, in which both transmission line branches (arms) have been replaced by BW-FW-transmission lines. The values L, C and d of these branches must be chosen so, that the values of one branch are proportional to the values of the other branch by the same coefficient, i.e. $L_2 = \xi L_1$, $C_2 = \xi C_1$ and $d_2 = \xi d_1$. Here ξ is the proportionality coefficient which must be the same for all the components of the two lines.

Since the parameters of the two lines are proportional, the matching frequencies (2.32) of the two lines are also proportional to each other: $\omega_1 = \xi^2 \omega_2$. The optimal performance of the phase shifter occurs between these frequencies, in which case one line operates in the forward wave region and the other one in the backward wave region. However, operation near the matching frequencies should be avoided, since imperfect matching conditions (2.31) may result in unstable phase shift behavior. The optimal operation frequency for the DLPS can be written

$$\omega_{\text{op}} = \sqrt{\omega_1 \omega_2} = \sqrt{\xi}\omega_2 = \frac{\omega_1}{\sqrt{\xi}} \,. \tag{2.33}$$

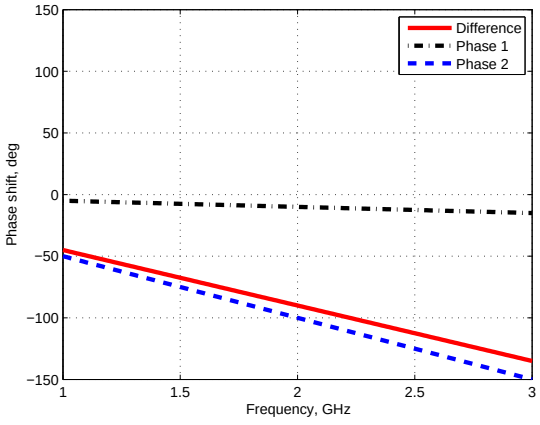

Figure 2.3: Phase behavior of a normal transmission line phase shifter.

In a transmission phase shifter which is based on normal transmission-line delay lines, the phase difference of the branches changes linearly as a function of the frequency, as seen in Figure 2.3.

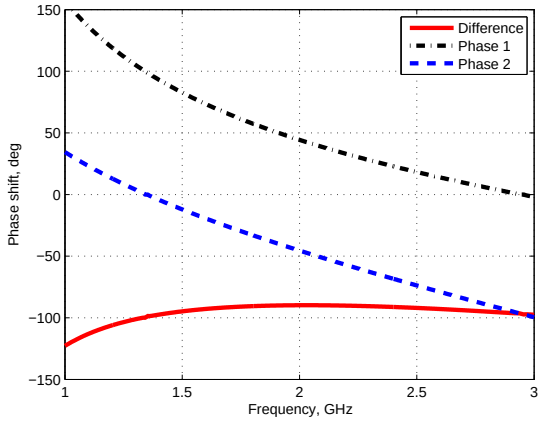

Figure 2.4: Phase behavior of a backward- forward wave transmission line phase shifter.

This leads to a very narrow bandwidth, on which the phase difference is acceptable. If the normal transmission lines are replaced by BW-FW-transmission lines, the phase curves behave as in Figure 2.4. In this case, the bandwidth is many times larger.

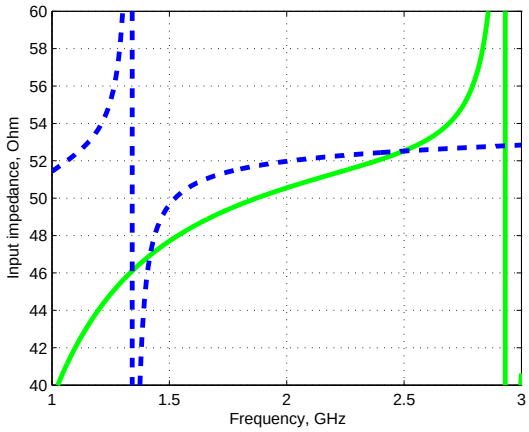

Figure 2.5: Impedance behavior of a backward- forward wave transmission line phase shifter. Impedance of branch 1 (green solid) and branch 2 (blue dashed).

While the phase stability of a DLPS is superior to that of a normal delay line phase shifter, the impedance matching is slightly worse. For a normal delay line phase shifter

the imput impedance would be almost constant in a wide range. Figure 2.5 shows the impedance curves of both branches of a DLPS. However, if the component values are chosen using the method described earlier, this variation in impedances is very close to $50\ \Omega$ at the operation frequency of around 2 GHz of this example.

3 Switchable Double-line Phase Shifter

Tunable or switchable phase shifters are very important for example for base station antenna arrays. In the double-line phase shifter (DLPS), the phase shift values are determined by the lumped inductance L, the lumped capacitance C and the propagation constant β. Tuning of these values would prove very complicated and difficult, especially for such high power applications as needed in base station antennas. Another way to adjust the phase shift is to make the DLPS switchable. This can be done by combining different forward-backward wave transmission-line sections by switches. In the following section this method is described in detail.

3.1 Design

There are two fundamental ways to realize the switchable DLPS design; the multiparallel and the sequential configuration. In the multiparallel configuration, the FW-BW transmission lines, which give the desired phase shift differences are, as the term suggests, in parallel (see Figure 3.1). The advantage of this design is the need of only two switches,

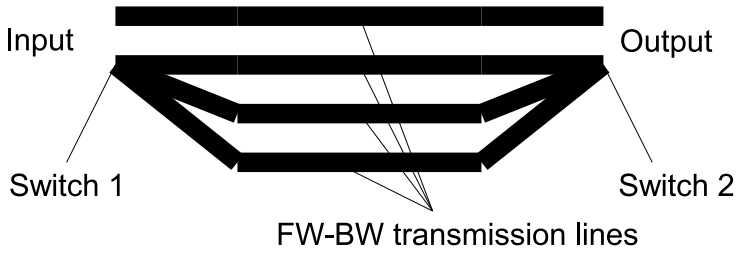

Figure 3.1: Parallel configuration alternative of the DLPS

which direct the incoming signal to the appropriate branches. The drawback is, however, that although in theory the parallel design with n branches can create $\sum_{k=1}^{n-1} k$ different phase shift values, in practice one needs n branches of FW-BW transmission lines for $n-1$ different phase shift values. For example, if one needs to have $75°$, $90°$ and $100°$ phase differences, then 4 branches are needed: The first one gives $0°$ phase shift from the

input to output, the second branch gives $75°$, and the third and fourth $90°$ and $100°$ phase shifts, respectively. In addition to the desired values, this phase shifter would also give $100° - 75° = 25°$, $90° - 75° = 15°$ and $100° - 90° = 10°$ phase differences. In some applications this might, of course, be of use. Another disadvantage of the multiparallel configuration is that with standard commercial lumped element sets, it is hardly possible to reach some phase shift combinations, since the values of the components in different branches neet to be proportional to each other and this is very difficult to achieve for more than two branches.

In the sequental configuration, there are only two FW-BW transmission line branches. The phase difference of these branches can be made to grow towards the end of them. Thus, by placing outputs to the right points on the lines, one can get the desired output phase differences. The outputs lie in series, connected with short sequences of FW-BW TLs, thus the name "sequental configuration". A simple schema of this design is shown

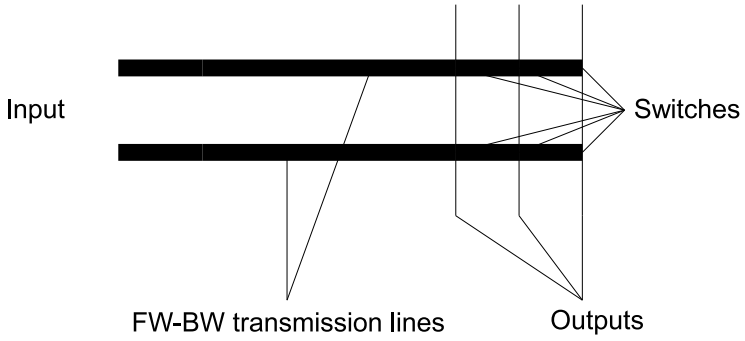

Figure 3.2: Series configuration alternative of the DLPS

in Figure 3.2. Compared to the parallel design, series design needs more switches and more complicated planar geometry for the output circuitry. The advantage is, however, that almost any set of phase shifts can be obtained with standard lumped elements.

The goal for the design of this *double-line phase shifter* (DLPS) was to have switchable outputs of $80°$, $90°$ and $100°$ frequency-stable phase difference at the frequency band of 1.92–2.17 GHz, which is used in the Universal Mobile Telecommunications System

(UMTS). To have a stable phase difference for wide band, backward-forward wave transmission lines in form of LC-loaded microstrip lines were used. The $80°$ position was achieved by three stages of $26.6°$ unit cells and the other two positions by additional $10°$ unit cells, one for $90°$ position and two for $100°$.

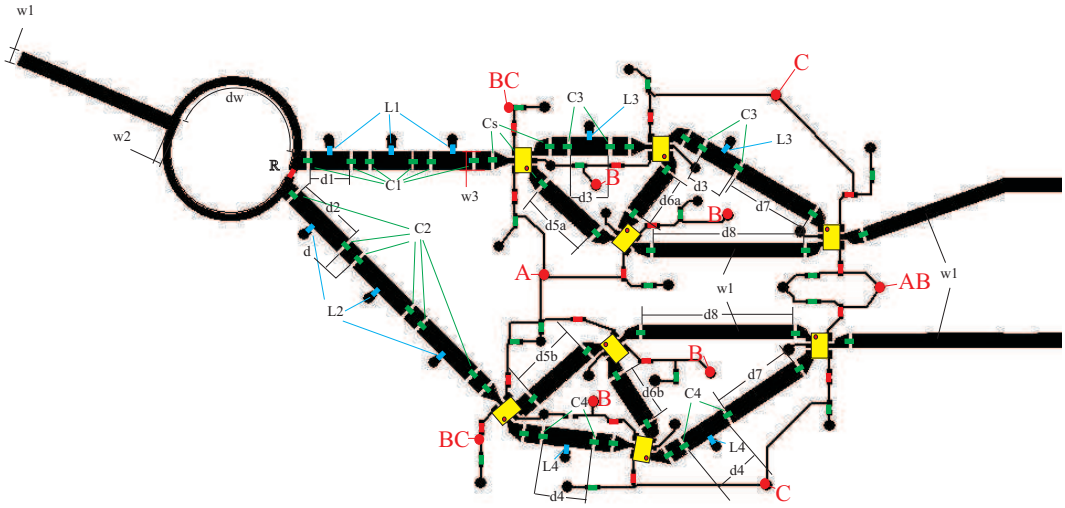

Figure 3.3: Schema of samples 1 and 2

Figures 3.3 and 3.4 show the schemas of two different modifications of the device. In the figure resistors are colored red, inductances blue, capacitances green and switches yellow. On the left is a Wilkinson power divider, which divides the input power to two branches of the DLPS. The input and output strip width w_1 is sized to have $50\ \Omega$ impedance. Since with the standard Murata components it is not possible to have perfect impedance matching ($Z = \sqrt{L/C}$) for input, this had to be compensated with a slightly different strip width w_3 in BW-FW parts of the device.

The letters in red indicate the bias voltage connections in the circuit. A refers to $80°$, B refers to $90°$ and C refers to $100°$. So, if one wants to have $80°$ output phase difference, then $V_{\text{on}} = 3.0\ \text{V}$ must be fed to all inputs with A in its marking (A and AB in the figure) and $V_{\text{off}} = 0.0\ \text{V}$ to all others. To have $90°$ phase difference, V_{on} must be fed to all inputs with marking B and V_{off} to others, and to get $100°$ phase difference, V_{on} must be fed to all inputs with marking C and V_{off} to others. Here V_{on} and V_{off} refer to switches' control

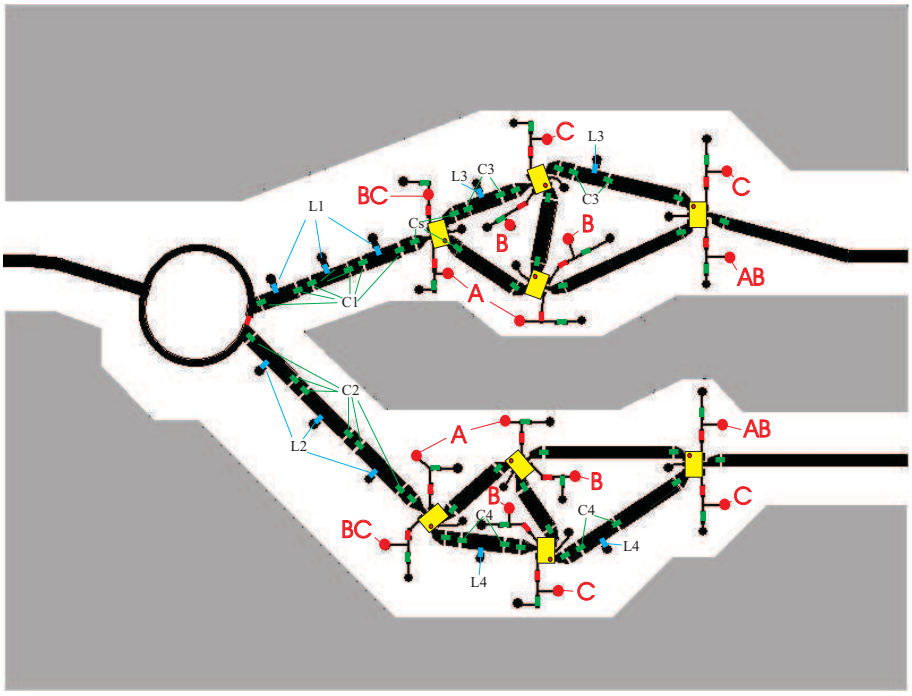

Figure 3.4: Schema of sample 3

voltage preferences.

The component values, substrate parameters and strip dimensions are portrayed in Table 3.1. The used switch type was M/A-Com's MASWSS0181, which was chosen due to its good power handling capacity, small size and easily solderable SOT-26 package.

3.2 Measurements

In search of better phase stability characteristics, three samples were manufactured. The measurements of each three switchable DLPS-samples were done with Agilent Technologies E8363A PNA series network analyzer, which was connected to the input and one of the two output ports of the DLPS. The other output port of the DLPS was connected to a $50\ \Omega$ matched load. To measure both S_{21} and S_{31} –parameters, the output connections had to be switched between the two ports. The measurement setup is shown in Figure 3.5.

Table 3.1: Component values, substrate parameters and microstrip dimensions

	Sample 1 and 2	Sample 3		All samples
w_1	1.89 mm	1.89 mm	C_1	4.7 pF GRM1555C1H4R7CZ01
w_2	1.06 mm	1.06 mm	C_2	6.8 pF GRM1555C1H6R8DZ01
w_3	2.34 mm	2.34 mm	C_3	5.6 pF GRM1555C1H5R6dZ01
d	2.0 mm	2.0 mm	C_4	6.8 pF GRM1555C1H6R8DZ01
d_1	5.18 mm	5.80 mm	C_s	100 pF GRM1555C1H101JZ01
d_2	9.06 mm	9.06 mm	L_1	5.6 nH LQP15MN5N6B02
d_3	5.04 mm	5.04 mm	L_2	8.2 nH LQP15MN8N2B02
d_4	6.42 mm	6.42 mm	L_3	7.5 nH LQP15MN7N5B02
d_{5a}	9.06 mm	10.26 mm	L_4	9.1 nH LQP15MN9N1B02
d_{5b}	9.06 mm	9.06 mm	ϵ_r	3.2
d_{6a}	7.03 mm	9.83 mm	h	0.787 mm
d_{6b}	7.03 mm	7.03 mm	$\tan\delta$	0.003
d_7	11.11 mm	11.11 mm	t	$30\ \mu m$
d_8	20.00 mm	20.00 mm	C_{block}	18 pF
d_w	25.15 mm	25.15 mm	R_{block}	1 kΩ

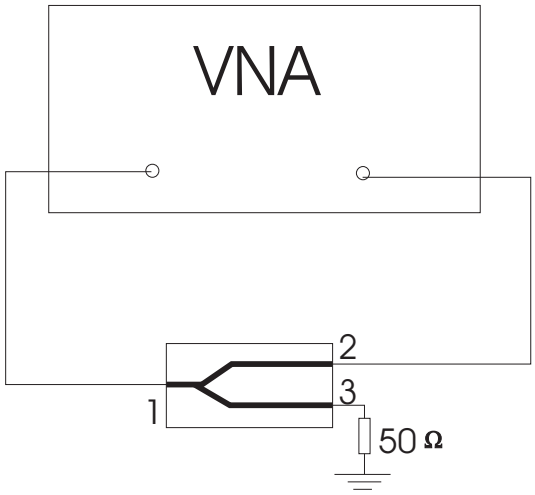

Figure 3.5: Measurement setup

3.2.1 Samples 1 and 2

The first two samples were identical with respect to each other and manufactured by VTT using the same layout. The used material was 0.8 mm thick TLC-32 substrate, with $\epsilon_r = 3.2$. A photo of sample 2 is shown in Figure 3.6.

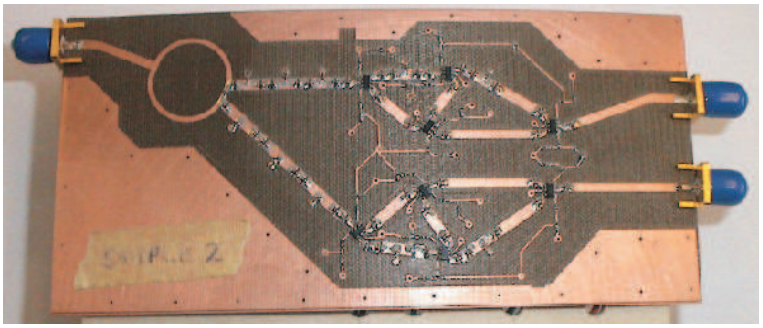

Figure 3.6: Sample 2

The measured and simulated reflection and transmission coefficients of Samples 1 and 2 are shown in Figure 3.7. In most cases the reflection at the UMTS band is lower than -20 dB, with an exception in the $80°$ position for Sample 2, in which the reflection is less than -15 dB. A possible cause for this exception may be a broken component or via in this circuit. The vias of the circuit board seemed to be very sensitive for even minor twisting, which may have happened during the connection of the circuit with the network

analyzer.

In Figures 3.8 — 3.10 one can see the measured phase differences of the two outputs of DLPS-samples 1 and 2, with the simulation results. On the right hand side of the three figures are the phase differences at the UMTS band, 1.92–2.17 GHz. It can be seen that the measured phase differences differ from the desired values a bit, especially in the $90°$ position, in which the difference is even $15°$. Also they vary with the frequency as much as $5°$, while in simulations this deviation was within $2°$. The effect of a possibly broken component or via is also visible in Figure 3.8, in which the performance of Sample 2 differs quite strongly from that of Sample 1.

It was suspected that the reason for such strong difference between the simulations and measurements was caused by the difficulties in predicting the performance of the switches. There was no S-parameter information available for them to be used in simulations, so some rather rough estimations had to be done when modeling these components. Therefore, to see if this assumption was correct, the switches of DLPS Sample 2 were replaced by copper wires. In Figure 3.11 one can see the performance of this DLPS with switches removed. The replacement copper wires had to be soldered for different positions to get each phase difference position.

These figures show much better agreement between the simulations and measurements. Not only are the results closer to the desired values, but also the formerly rather large deviation within the UMTS range is now much milder. In the $90°$ and $100°$ positions there is around $7°$–$8°$ difference between the simulated and the measured results which was assumed to be caused by the increase in the strip thicknesses due to tin used in soldering of components. This effect is relatively stronger in the shorter branch of the DLPS, which alters the relative phase behavior of the branches. Also other nonidealities in design (simulations never portray real world perfectly), production (component and etching tolerances) and measurement setup may have caused this.

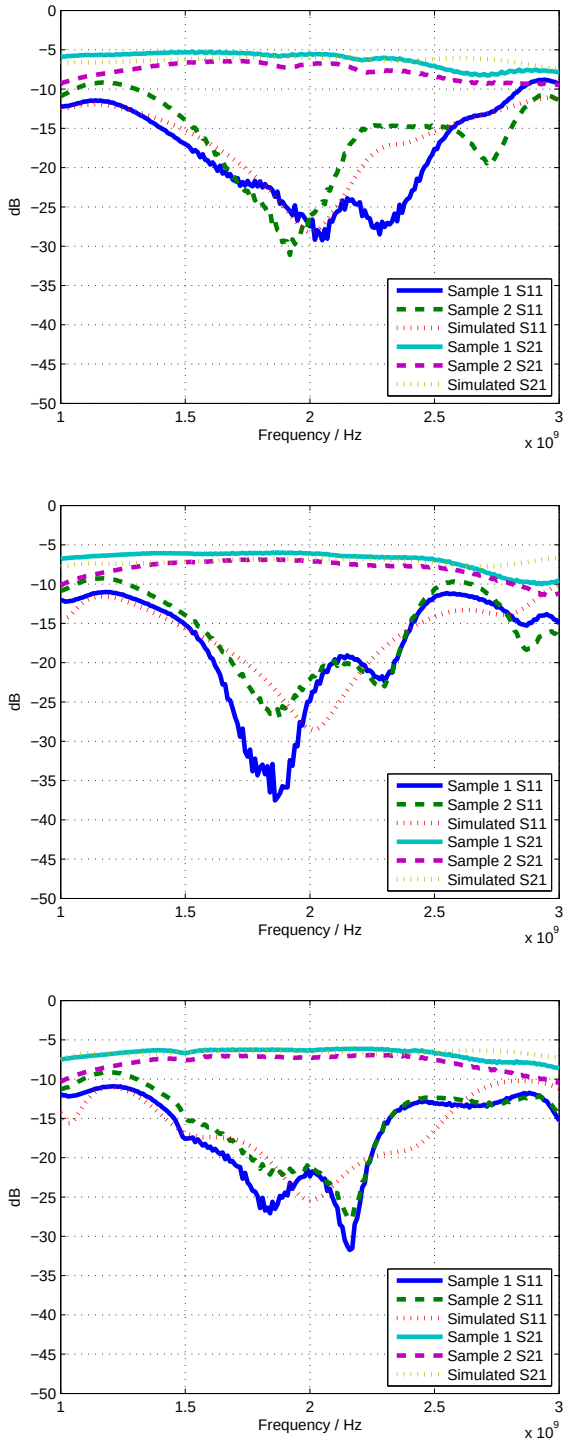

Figure 3.7: Reflection and transmission coefficients of samples 1 and 2 at $80°$ (upper), $90°$ (middle) and $100°$ (lower) positions

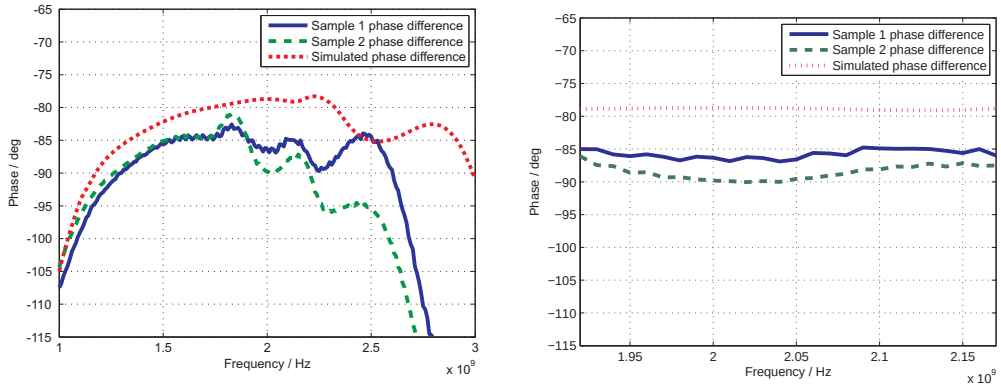

Figure 3.8: Phase differences of Samples 1 and 2 at 80° position

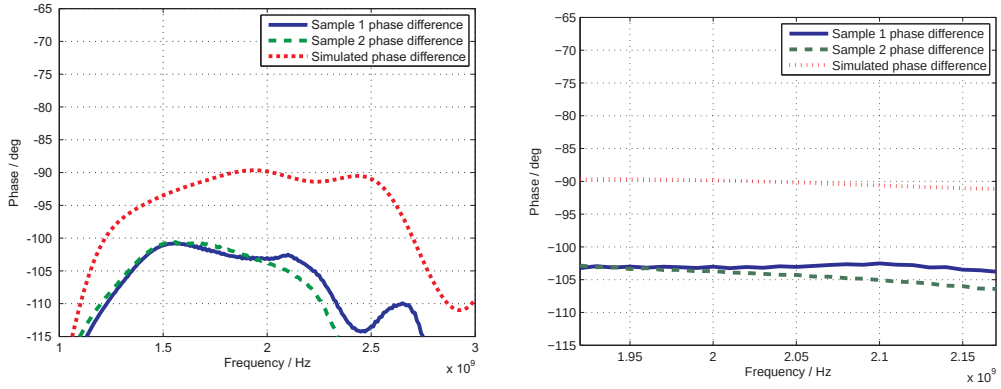

Figure 3.9: Phase differences of Samples 1 and 2 at 90° position

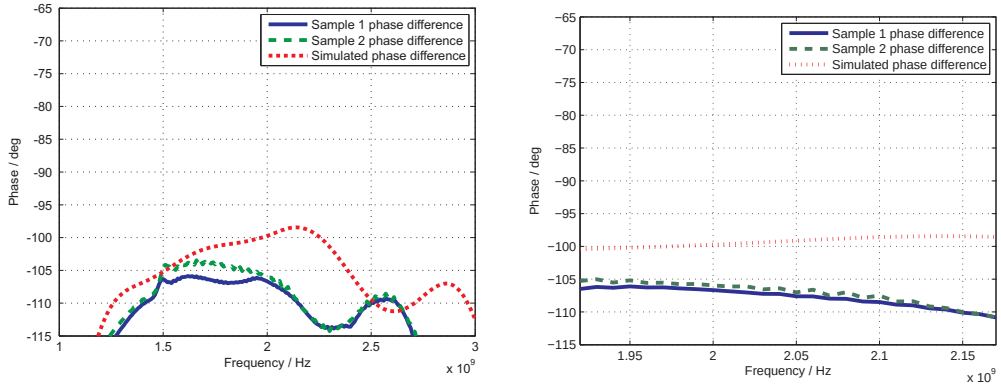

Figure 3.10: Phase differences of Samples 1 and 2 at 100° position

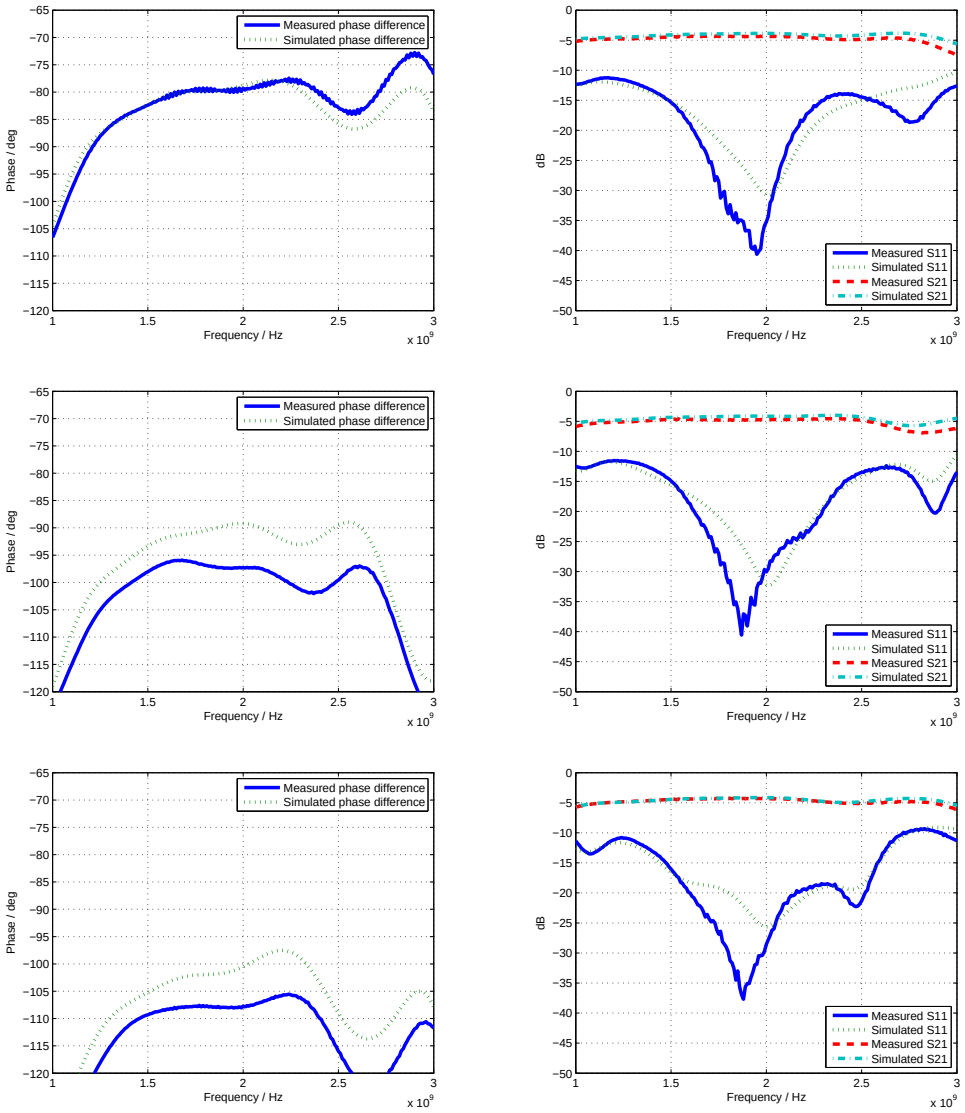

Figure 3.11: Circuit performance without switches

3.2.2 Sample 3

In order to improve the performance of the DLPS, yet another sample was designed. Modifications in this design included changes in some microstrip lengths to counter the effect of the switches, a ground plane between the two branches to reduce possible coupling, and all switch biases brought as directly as possible through the substrate to the switches, without any DC-routings on the top of the substrate (see Figure 3.12).

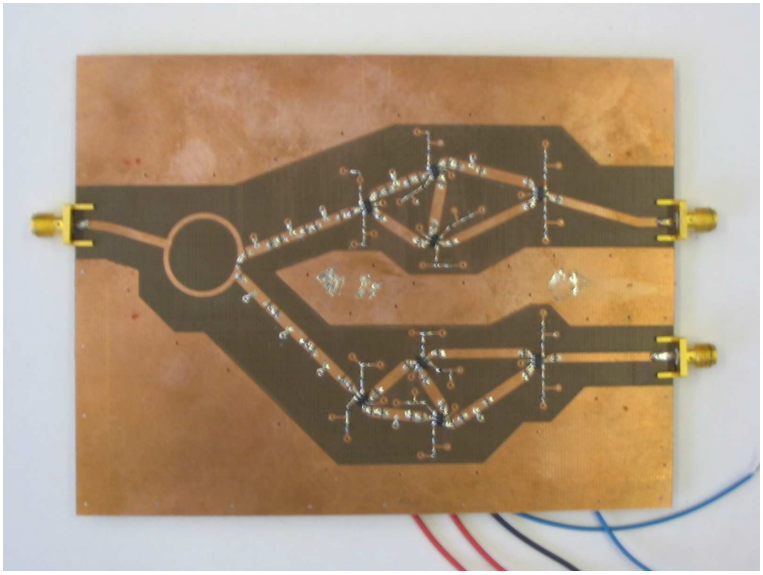

Figure 3.12: Sample 3

This sample was etched in Micronova but the components were soldered by the author at TKK, Laboratory of Applied Electronics. The measurement setup was the same as before. The performance of Sample 3 is shown in Figures 3.13–3.16. It seems that the phase differences are now slightly closer to the wanted values but for some reason $80°$ and $90°$ positions seem to be over corrected and are now $10°$ offset to the opposite direction. This is most likely to be due to considerably smaller amounts of soldering paste used in Sample 3 than in Samples 1 and 2, or due to other changes made into the layout of the circuit. Also, different types of 100 pF blocking capacitors were used in sample 3 (Taiyo Yuden UMK105CH101JW) than in samples 1 and 2 (Murata GRM1555C1H101J), simply because of finite supply of both component types. Otherwise the performance is

quite close to that of Samples 1 and 2.

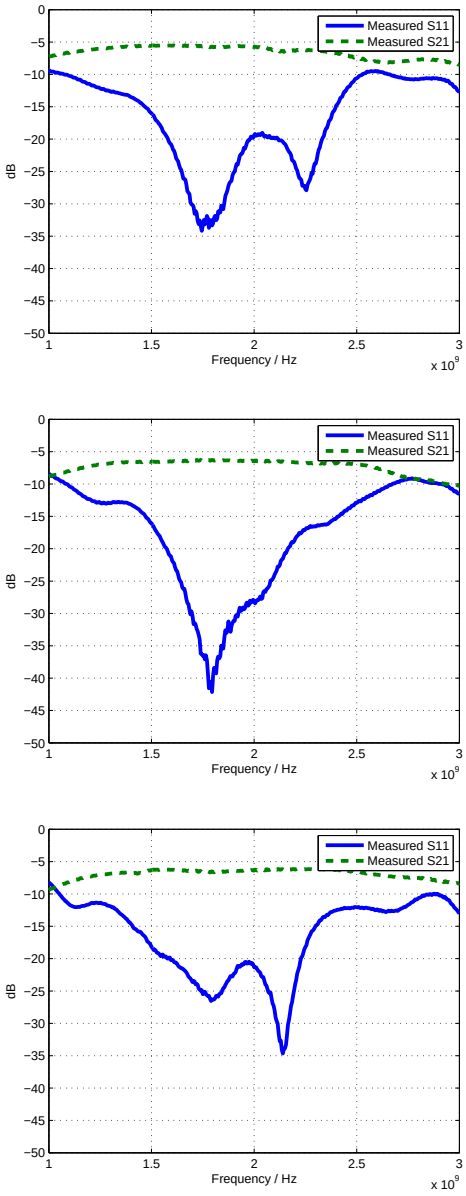

Figure 3.13: Reflection and transmission coefficients of sample 3 at $80°$ (upper), $90°$ (middle) and $100°$ (lower) positions

3.3 Conclusions

In this work we successfully created a phase shifter utilizing the advantages of backward-forward-wave transmission lines. These advantages include compact size, frequency sta-

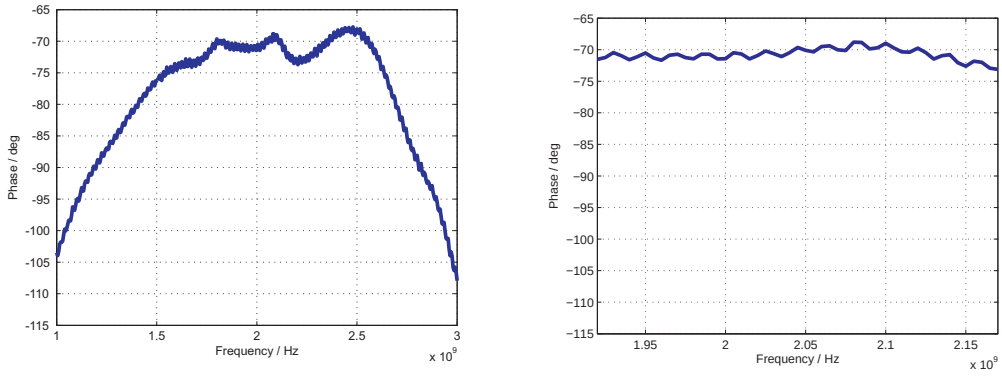

Figure 3.14: Phase difference of Sample 3 at $80°$ position

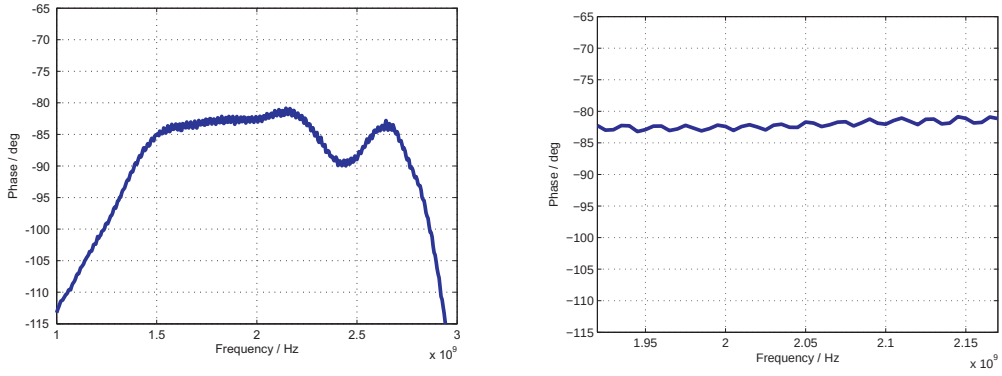

Figure 3.15: Phase difference of Sample 3 at $90°$ position

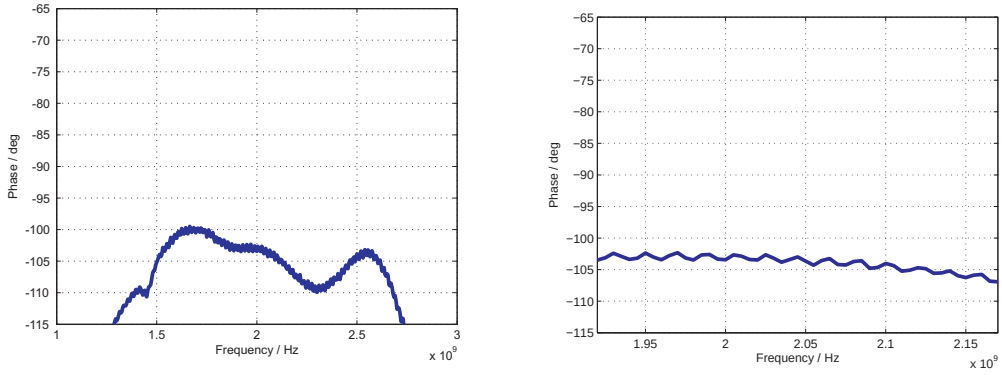

Figure 3.16: Phase difference of Sample 3 at $100°$ position

bility and rather simple manufacturing process.

It seems that the main problem in designing such switchable DLPS is the inability to accurately estimate the behavior of the switches in simulations. However, with enough information on these components, it is certainly possible to produce a device with good enough performance. Also, the design is very sensitive to manufacturing imperfections, but this problem can be dealt by a few iterations for a given manufacturing process. The phase deviation at UMTS band for the prototypes is $2°$–$5°$, while for a traditional transmission line phase shifter this would be about $10°$, which is a clear improvement. Reflection coefficient at UMTS band is usually less than -20 dB and resistive losses, of which most happen in switches, are about 4 dB (2 dB when switches are replaced with copper wires). Note, that the additional 3 dB drop in transmission coefficients in the figures comes from power division. Overall, it looks like the design is certainly promising with regards to further developing, and even with the problems with the switches, the designed prototypes perform reasonably well. The main results of this work have been published in [1] and are protected by a patent.

4 Forward- Backward-wave Balun

4.1 Introduction

A *balun* is a device, which is used to make a transition between *an unbalanced* and *a balanced transmission line*. Also the impedance may be changed during this operation. Unbalanced line is a transmission line consisting of a signal line and a ground. For example, coaxial cable and microstrip line are unbalanced transmission lines. Balanced line, such as twin-lead, consists of two similar conductors, which have equal impedances to the ground.

Delay line type baluns are a large class of baluns. They are simple in design, but have a drawback of rather narrow bandwidth. A schematic of a half-wavelength delay line type balun is shown in Figure 4.1. The unbalanced input is transformed into balanced output by separating the two output lines with a transmission line of length $\frac{\lambda}{2}$. This half-wavelength

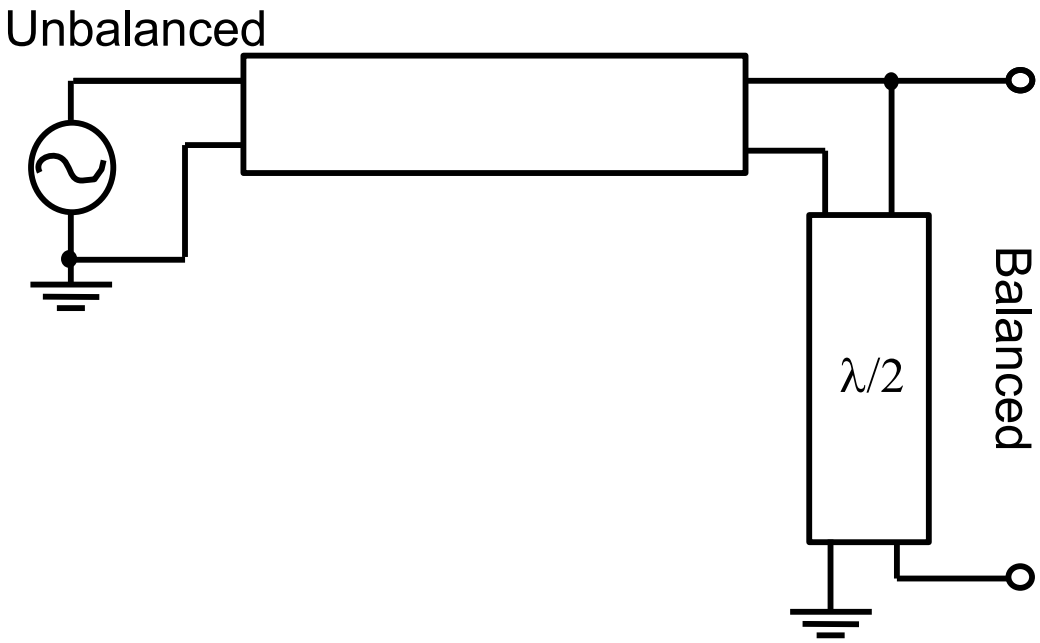

Figure 4.1: Schematic of a half-wavelength delay line balun

delay line produces a $180°$ phase difference between the output ports thus resulting in balanced output.

4.2 Design

The double line phase shifter, DLPS, gives an idea to use forward- backward-wave transmission line (FW-BW-TL) pieces to convert unbalanced input to balanced output. In Figure 4.2 can be seen the schematic of such balun. The FW-BW-TL pieces of electrical length $\frac{\lambda}{4}$ and $-\frac{\lambda}{4}$ create this needed $180°$ phase difference between the output ports.

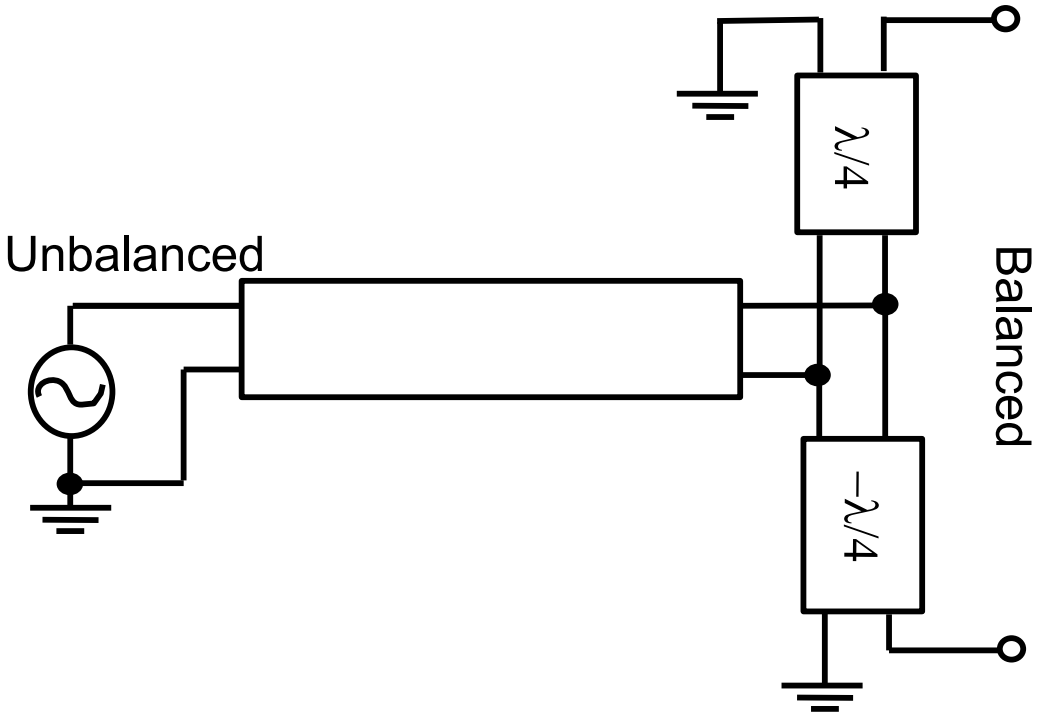

Figure 4.2: Schematic of a forward- backward-wave balun

Figure 4.3 shows the circuit diagram of the FW-BW-TL balun, designed to work at 2 GHz. The component values are chosen by using equations (2.32) and (2.33), and are shown in Table 4.1. Note that in order to keep the circuit diagram simpler, the capacitances of the adjacent unit cells are merged together. Thus the values of the capacitances in Table 4.1 are one half of the values obtained from the equations. w_{in} is the microstrip width before the T-junction on the left and w_0 is the microstrip width elsewhere. The load on the right is a 73 Ω resistor as a simplified model of a half-wave dipole antenna, depicting only its radiation resistance.

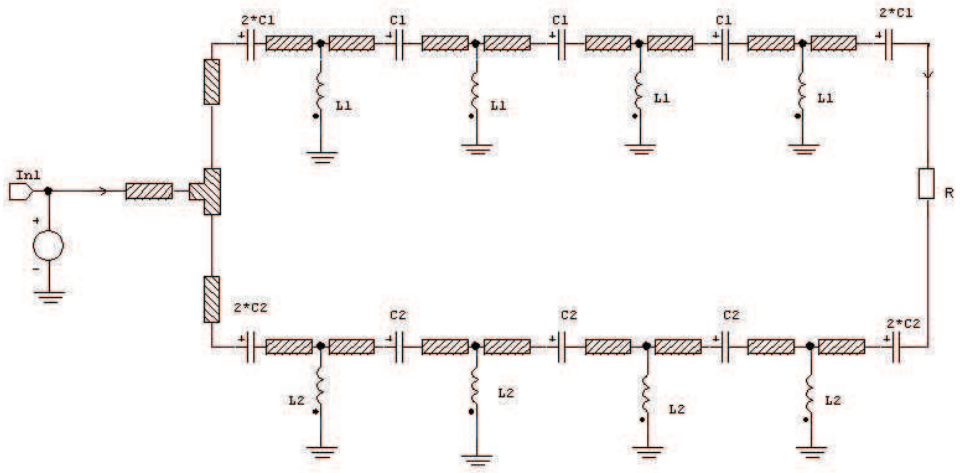

Figure 4.3: The circuit diagram of the forward- backward-wave balun

Table 4.1: Component values, substrate parameters and microstrip dimensions of the balun

$C_1 = 1.80$ pF	$L_1 = 6.00$ nH	$d_1 = 3.14$ mm
$C_2 = 3.60$ pF	$L_2 = 12.00$ nH	$d_2 = 6.28$ mm
$\epsilon_r = 2.33$	$h = 0.787$ mm	$\rho_n = 0.725\ \Omega$m
$\tan\delta = 0.001$	$t = 30\ \mu$m	
$w_0 = 1.91$ mm	$w_{\text{in}} = 2.3$ mm	

4.3 Simulation Results

The designed circuit was simulated with APLAC circuit simulator. When simulating the circuit with a simple resistor as a load, as shown in Figure 4.3, an unexpected resonance occurred at the center of the intended operating frequency range of the device, i.e. 2 GHz (see Figure 4.4).

This behavior is likely to occur due to the fact that the circuit forms a resonating ring which by design is optimized to work at the frequency of 2 GHz. To work around this phenomenon, the resistive load was split into two grounded resistors thus breaking the closed circuit path and preventing possible resonances. Note that a dipole antenna does not form a closed circuit path between the two balun branches either.

In Figure 4.5 we show the performance of the FW-BW-balun with separated loads. For comparison, also the performance of a simple delay line balun is shown in Figure 4.6.

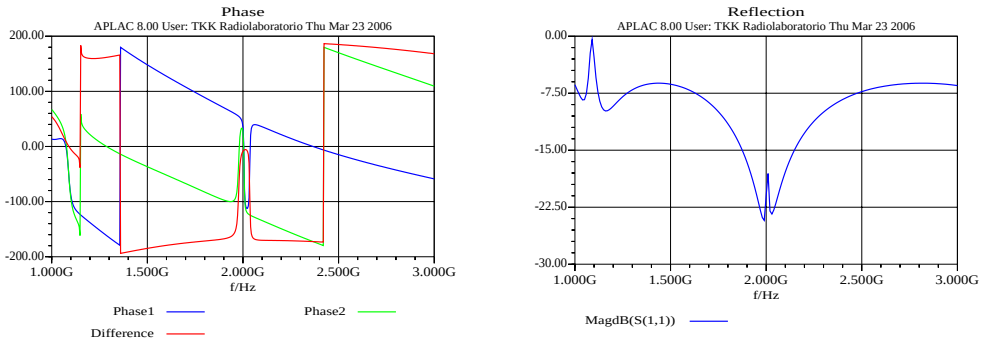

Figure 4.4: FW-BW-balun's phase curve (left) and reflection coefficient curve (right).

From the left side figures one can see that the FW-BW-balun gives a constant $180°$ phase difference (meaning balanced output) on a large frequency range (red line), whereas for the delay line balun the output phase difference varies as a function of frequency. On the other hand, on the right side figures can be seen that the traditional delay line phase shifter has more stable reflection coefficient as a function of frequency. Nevertheless, the reflection coefficient of the FW-BW-balun is also reasonably good.

4.4 Conclusions

Despite having problems with some load types, the backward- forward-wave balun has clear advantages over traditional planar balun types especially with its stable phase behavior on a wide frequency range. Also its size can be made equivalent or even smaller than the size of a half wavelength balun. The only drawback of this design seems to be

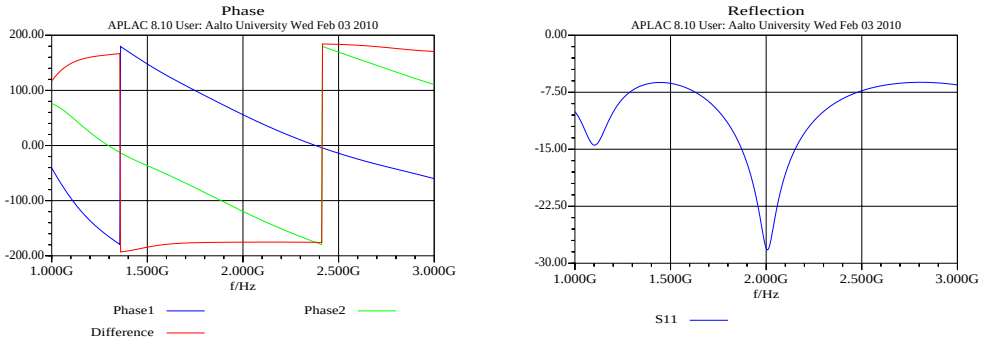

Figure 4.5: FW-BW-balun's phase curve (left) and reflection coefficient curve (right). Separated load.

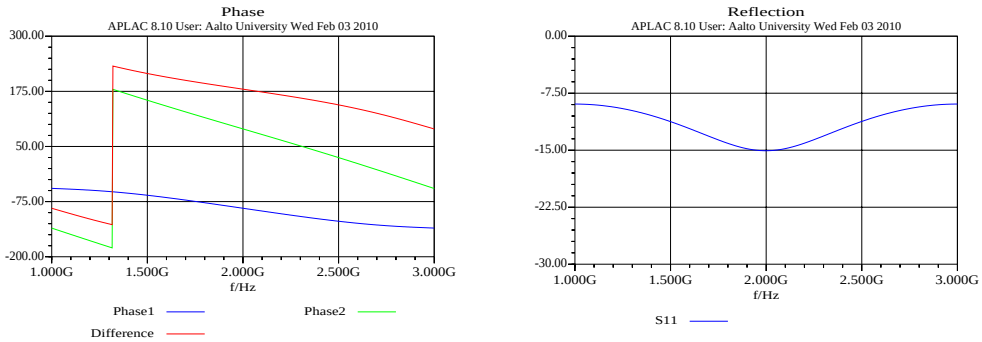

Figure 4.6: Delay line balun's phase curve (left) and reflection coefficient curve (right).

the narrow impedance bandwidth.

However, for applications which require a stable phase behavior at wide band, this balun type could be a good choice.

A Matlab codes to calculte the phase shifter parameters

Codes and comments are by Ph.D. Mikhail Lapine.

A.1 tldf.m

```
%% ============================
%% Main unit for DLPS analysis
%% ============================
%
clear all
global ZZ K0 L0 C0 X nabor fop L1 C1 L2 C2
%
% ========================
% ========================
% User-defined parameters:
% -------------------
% Main tuning factor:
% -------------------
X = 1.5;
% (proportionality coefficient between two lines)
% -------------------------------
% Initial tuning L, C and d values
% -------------------------------
scal = 2;
% scaling of the lumped component values:
% C with respect to 2pF and L with respect to 5nH
% (so that L/C ratio is always matched to 50 Ohm)
% ----------------------------------------
```

```
% Swith between initial and predefined set:
% ----------------------------------------
nabor = 80;
% (required for "xlc.m" module
% value 0: specified L and C, calculated using "scal" and
% "X" values 80 or 100: pre-defined L and C, taken from
% Murata set (optimized for three-stage 80 or 100 deg
% shifters) value 45: pre-defined Murata L and C to have
% 45 deg shift per stage any further sets can be added to
% "xlc.m" module and called here using corresponding "nabor"
% value
% ------------------------------------
% Tl length tuning for predefined sets:
% ------------------------------------
% NOTE: parameters of this section work only with predefined
% sets! if "nabor = 0", they are overwritten by calculated
% ideal value
%
tld = 6.95; % mm
% total length of one microstrip segment (two segments per
% section), mm refers to the line-1; line-2 will be
% automatically calculated
%
ZZ = 50; % Ohm
% wave impedance of ALL microstrip segments (default = 50 Ohm)
%
% --------------
% Other settings:
```

```
% ---------------
Ugl = 80;
% total intended phase shift (degrees),
% used only to calculate number of stages
%
fop = 2e9;
% approximate operational frequency, Hz
% can be used to "move" the operational range
%
risuj = [1,1,1];
% this is whether to plot frequency dependence of (1,2,3):
% 1) phase shifts per unit cell
% 2) input impedances of two lines
% 3) reflection from each line in dB
% value 1 is to have a figure, any other value is to omit
% that figure
% ------------------------------
% End of user-defined parameters
% ==============================
% ==============================
%
% -------------------------
% Default L0 and C0 values:
%
L0 = scal*5e-9;      % 5 nanoHenry
C0 = scal*0.002e-9;  % 2 picoFarad
K0 = tld/3e11; % is used only for predifined sets
%
```

```
% --------------------
% Calling "xlc" module
%
xlc
%
% ------------------------------
% UMTS range with two subranges:
frl  = 1.92e9;
frll = 1.98e9;
frhh = 2.11e9;
frh  = 2.17e9;
%
%---------------------------
% Phase shifts in UMTS range
[faz1l,faz2l,dfl] = fazer(frl,X);
[faz1ll,faz2ll,dfll] = fazer(frll,X);
[faz1hh,faz2hh,dfhh] = fazer(frhh,X);
[faz1h,faz2h,dfh] = fazer(frh,X);
[faz1c,faz2c,dfc] = fazer(2e9,X);

% Additional calculations
stages = abs(Ugl/dfc);
razval = stages*abs(dfl - dfh);
razval1 = stages*abs(dfll - dfl);
razval2 = stages*abs(dfhh - dfh);
% -------------------------

% Impedance deviations in in UMTS range
```

```
[vo1,vo2,Zin1l,Zin2l,vo5,vo6] = ampler(frl,X);
[vo1,vo2,Zin1h,Zin2h,vo5,vo6] = ampler(frh,X);
Zinmin = min([Zin1l,Zin2l,Zin1h,Zin2h]);
Zinmax = max([Zin1l,Zin2l,Zin1h,Zin2h]);

% ============================
% OUTPUT  SCREEN  PREPARATION
% ############################

% For phase shifts:
%
perstag = strcat('Phase shift per one stage =',num2str...
    (abs(dfc)),' degrees');
stag = strcat('Stages number (for_ ',num2str(Ugl),' ...
    deg total shift) =',num2str(stages));
vyvod = strcat('overall =',num2str(razval),', 1st ...
    subrange =',num2str(razval1),', 2nd subrange =',...
    num2str(razval2));
disp(perstag);
disp(stag);
disp('Phase deviations within UMTS range, degrees:');
disp(vyvod);

% For DLPS parameters:
%
propco = strcat('Proportionality between two lines, ...
X=',num2str(X));
pary1 = strcat(' L1=',num2str(L1*1e9),'nH, C1=',...
```

```
    num2str(C1*1e12),'pF, d1=',num2str(K0*3e11),'mm');
pary2 = strcat(' L2=',num2str(L2*1e9),'nH, C2=',...
    num2str(C2*1e12),'pF, d2=',num2str(K0*3e11*X),'mm');
disp(propco);
disp(pary1);
disp(pary2);

%% not used % Lower cut-off frequency (approximate!):
%% not used % fcut = 1/(4*pi*(L1*C1)^0.5);
%% not used % disp(strcat('Cut-off frequency =',...
%% not used & num2str(fcut*1e-9),' GHz'));
%%
%% not used % f1 = fop*sqrt(X);
%% not used % zerocros1 = strcat(' f1=',num2str...
%% not used % (f1*1e-9),'GHz');
%% not used % zerocros2 = strcat(' f2=',num2str...
%% not used % (f1*1e-9/X),'GHz');
%% not used % disp(zerocros1);
%% not used % disp(zerocros2);


% Impedances
%
koni = strcat('Z min=',num2str(Zinmin),', Z max=',...
    num2str(Zinmax),', difference =',num2str...
    (Zinmax - Zinmin),' (Ohms)');
disp('Input impedance deviations:');
disp(koni);
```

```
% ==============================
% PLOTS for Frequency dependence
% ++++++++++++++++++++++++++++++
%
% Frequency dependence: "NF" points in range from
% "flo" to "fhi" Hz
%
NF = 1000;
for n = 1:NF
    flo = 1e9;
    fhi = 3e9;
    fstep = (fhi - flo)/(NF - 1);
    freq(n) = flo + (n-1)*fstep;
    omg(n) = 2*pi*freq(n);

    [faza1(n),faza2(n),razfaz(n)] = fazer(freq(n),X);

    [SWR1(n),SWR2(n),Zin1(n),Zin2(n),Gam1(n),Gam2...
     (n)] = ampler(freq(n),X);

end
%
% ----------------------------
% 1) phase shifts per unit cell

if risuj(1) == 1
```

```
    figure(13)
    plot(freq*1e-9,razfaz,'--r')
    hold on
    plot(freq*1e-9,faza1,'--g')
    plot(freq*1e-9,faza2,'--b')
    title('Line1 - green, line2 - blue, phase shift - red')
    xlabel('Frequency, GHz')
    ylabel('Phase shifts, degrees')
    %
    % OPTIONAL: vertical lines for UMTS range visualization:
    line([frl*1e-9 frl*1e-9],[-90 90],'Color','k')
    line([frh*1e-9 frh*1e-9],[-90 90],'Color','k')
    %hold off

end

% --------------------------------
% 2) input impedances of two lines

if risuj(2) == 1

    figure(30)
    plot(freq*1e-9,Zin1,'--g')
    hold on
    plot(freq*1e-9,Zin2,'--b')
    title('Line1 - green, line2 - blue')
    xlabel('Frequency, GHz')
    ylabel('Impedance, Ohm')
```

```
    %
    % OPTIONAL: vertical lines for UMTS range visualization:
     line([frl*1e-9 frl*1e-9],[25 75],'Color','k')
     line([frh*1e-9 frh*1e-9],[25 75],'Color','k')

end

% -------------------------------------
% 3) reflection at the two inputs in dB

if risuj(3) == 1

    figure(31)
    plot(freq*1e-9,20*log10(Gam1),'-g')
    hold on
    plot(freq*1e-9,20*log10(Gam2),'-b')
    title('Line1 - green, line2 - blue')
    xlabel('Frequency, GHz')
    ylabel('Reflection, dB')
    %
    % OPTIONAL: vertical lines for UMTS range visualization:
    % line([frl*1e-9 frl*1e-9],[-50 0],'Color','k')
    % line([frh*1e-9 frh*1e-9],[-50 0],'Color','k')

end

%% END of file
```

A.2 ampler.m

```
function [swr1,swr2,zir1,zir2,gam1,gam2] = ampler(ff,x)

global L1 C1 L2 C2 K0 ZZ

FF = ff;
K1 = K0;
K2 = x*K0;

[H1,Z1] = hip(FF,K1,L1,C1);
[H2,Z2] = hip(FF,K2,L2,C2);

am1 = abs(H1);
am2 = abs(H2);

zir1 = real(Z1);
zir2 = real(Z2);
zim1 = imag(Z1);
zim2 = imag(Z2);

gam1 = abs(50 - zir1)/(50 + zir1);
gam2 = abs(50 - zir2)/(50 + zir2);

swr1 = (1 - gam1)/(1 + gam1);
swr2 = (1 - gam2)/(1 + gam2);
```

A.3 fazer.m

```
function [fa1,fa2,df] = fazer(ff,x)
```

```
global L1 C1 L2 C2 K0 ZZ

FF = ff;
K1 = K0;
K2 = x*K0;

[H1,void1] = hip(FF,K1,L1,C1);
[H2,void2] = hip(FF,K2,L2,C2);

am1 = abs(H1);
fa1 = 180/pi*angle(H1);
am2 = abs(H2);
fa2 = 180/pi*angle(H2);
df = fa2 - fa1;

%%[o1,o2,o3] = [fa1,fa2,df];
```

A.4 hip.m

```
function [otvet,dopot] = hip(f,k,l,c)

global ZZ

w = 2*pi*f;

bd = w*k;

QC = [1, 1/(i*w*2*c); 0, 1];
```

```
QL = [1, 0; 1/(i*w*l), 1];
TL = [cos(bd), i*ZZ*sin(bd); i*sin(bd)/ZZ, cos(bd)];

Q = QC*(TL*(QL*(TL*QC)));
%% Q =  QC*(QL*QC); % ..... testing only backward
%% Q =  TL*TL; % ..... testing only forward
a = Q(1,1);
b = Q(1,2);
c = Q(2,1);
d = Q(2,2);

discr = ((d - a)^2 + 4*b*c)^0.5;
%% Zin1 = ((a - d)^2 + discr)/2/c;
%% Zin2 = ((a - d)^2 - discr)/2/c;
Zin1 = ((a - d) + discr)/2/c;
Zin2 = ((a - d) - discr)/2/c;

if real(Zin1)>=0
    Zin = Zin1;
else if real(Zin2)>=0
        Zin = Zin2;
    else
        beda=strcat('Trouble with Zin at_',num2str(w),...
         '_2*pi*GHz');
        disp(beda);
    end
end
```

```
otvet = 1/(a + b/Zin);
dopot = Zin;
```

B Dispersion Equation in FW-BW-TL

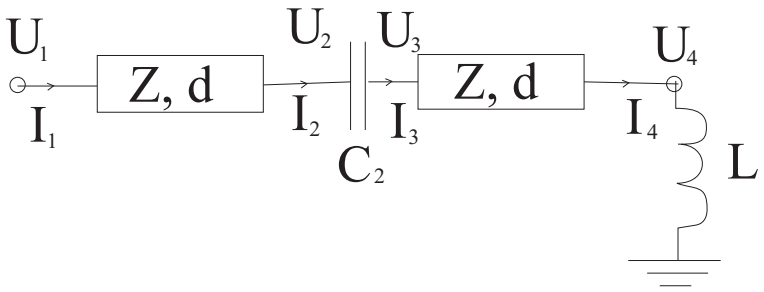

Figure B.1: Voltages and currents in unit cell

The transmission matrices for the normal transmission line, the series capacitor and the shunt inductor in the unit cell of FW-BW-TL, seen in Fig. B.1 can be written

$$A_{\mathrm{TL}} = \begin{pmatrix} \cos\beta_{\mathrm{TL}}d & jZ\sin\beta_{\mathrm{TL}}d \\ \frac{j\sin\beta_{\mathrm{TL}}d}{Z} & \cos\beta_{\mathrm{TL}}d \end{pmatrix} = \begin{pmatrix} A & B \\ C & D \end{pmatrix} , \tag{B.1}$$

$$A_{\mathrm{C}} = \begin{pmatrix} 1 & \frac{1}{j\omega C_2} \\ 0 & 1 \end{pmatrix} \tag{B.2}$$

and

$$A_{\mathrm{L}} = \begin{pmatrix} 1 & 0 \\ \frac{1}{j\omega L} & 1 \end{pmatrix} , \tag{B.3}$$

respectively. Here C_2 is the combination of two capacitors of value C in series. From these matrices and Fig. B.1 the following equations can be written:

$$\begin{pmatrix} U_1 \\ I_1 \end{pmatrix} = \begin{pmatrix} A & B \\ C & D \end{pmatrix} \begin{pmatrix} U_2 \\ I_2 \end{pmatrix} \tag{B.4}$$

$$\begin{pmatrix} U_2 \\ I_2 \end{pmatrix} = \begin{pmatrix} 1 & \frac{1}{j\omega C_2} \\ 0 & 1 \end{pmatrix} \begin{pmatrix} U_3 \\ I_3 \end{pmatrix} \tag{B.5}$$

$$\begin{pmatrix} U_3 \\ I_3 \end{pmatrix} = \begin{pmatrix} A & B \\ C & D \end{pmatrix} \begin{pmatrix} U_4 \\ I_4 \end{pmatrix} . \tag{B.6}$$

Thus, can be written

$$\begin{pmatrix} U_1 \\ I_1 \end{pmatrix} = \begin{pmatrix} A & B \\ C & D \end{pmatrix} \begin{pmatrix} 1 & \frac{1}{j\omega C_2} \\ 0 & 1 \end{pmatrix} \begin{pmatrix} A & B \\ C & D \end{pmatrix} \begin{pmatrix} U_4 \\ I_4 \end{pmatrix} . \tag{B.7}$$

From this matrix equation I_4 can be derived:

$$I_4 = \frac{j\omega C_2}{j\omega(A+D)BC_2 + AD} U_1 - \frac{j\omega(A^2+BC)C_2 + AC}{j\omega B(A+D)C_2 + AD} U_4 = SU_1 + KU_4 . \tag{B.8}$$

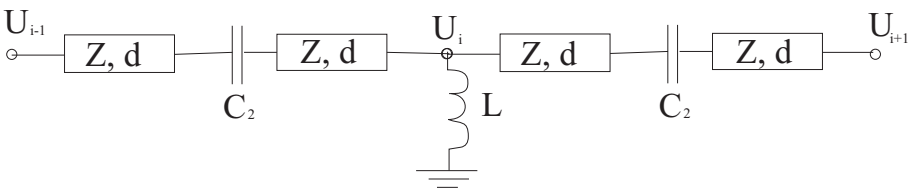

Figure B.2: Adjacent unit cells

From Fig. B.2 and Eq. (B.8) it can be seen, that

$$S \cdot U_{i-1} + S \cdot U_{i+1} + 2K \cdot U_i = \frac{U_i}{j\omega L} \ . \tag{B.9}$$

If the voltage is time-harmonic, (B.9) can be written as

$$S \cdot U_i (e^{+j2\beta d} + e^{-j2\beta d}) + 2K \cdot U_i = \frac{U_i}{j\omega L} \ , \tag{B.10}$$

$$\cos 2\beta d = \frac{1}{j2\omega LS} - \frac{K}{S} \ . \tag{B.11}$$

References

[1] T. Mynttinen, M. Lapine, J. Säily, I.S. Nefedov, and S.A. Tretyakov: *Microwave devices with enhanced phase-compensation principle*, Proc. EuCAP 2006, Nice, France, November 6-10, 2006 (ESA SP-626, October 2006)

[2] V.G. Veselago, *The electrodynamics of substances with simultaneously negative values of ϵ and μ*, Soviet Phys Uspekhi 10 (1968)

[3] J.B. Pendry, *Negative refraction makes a perfect lense*, Physical Review Letters, 85:3966, 2000

[4] A. Lehto, A. Räisänen: *RF- ja mikroaaltotekniikka*, Otatieto Oy, 7. painos, 2002

[5] B. M. Schiffman: *A New Class of Broad-Band Microwave 90-Degree Phase Shifters*, IRE Transactions on Microwave Theory and Techniques, April 1958

[6] J. P. Shelton, J. A. Mosko: *Synthesis and Design of Wide-Band Equal-Ripple TEM Directional Couplers and Fixed Phase Shifters*, IEEE Transactions on Microwave Theory and Techniques, Vol. MTT-14, No. 10, October, pp. 462–473, 1966

[7] D. Kim, Y. Choi, M. G. Allen, J. S. Kenney, D. Kiesling: *A Wide-Band Reflection-Type Phase Shifter at S-Band Using BST Coated Substrate*, IEEE Transactions on Microwave Theory and Techniques, Vol. 50, No. 12, pp. 2903–2909, December 2002

[8] M. Antoniades, G. Eleftheriades: *Compact Linear Lead/Lag Metamaterial Phase Shifters for Broadband Applications*, IEEE Antennas And Wireless Propagation Letters, Vol. 2, 103-106, 2003

[9] I. S. Nefedov, S. A. Tretyakov: *On Potential Applications of Metamateroaös for the Design of Broadband Phase Shifters*, Microwave and Optical Technol. Lett., Vol. 45, Issue 2, 98, 2005

[10] A. Räisänen, A. Lehto, *Radiotekniikan perusteet*, Otatieto Oy, 10. painos, 2001

[11] I. Lindell, *Aaltojohtoteoria*, Otatieto Oy, 2. painos, 1997